

Published in *Geophysical Research Letters*, 28, 4315-4318, 2001. Copyright 2001 American Geophysical Union. Further reproduction or electronic distribution is not permitted.

Modeling broadscale deformation in northern California and Nevada from plate motions and elastic strain accumulation

Mark H. Murray¹, Paul Segall

Department of Geophysics, Stanford University, California

Abstract

We present a first-order method for modeling broadscale deformation consistent with both plate tectonic motions and elastic strain accumulation on plate boundary faults. Interseismic deformation is assumed to be a superposition of long-term rigid-body motions between faults, defined by angular velocities of spherical plates, and backslip on shallow locked portions of faults in an elastic half-space. This method is applied to 1993–2000 continuous GPS data from 35 sites in a profile from the San Francisco Bay area, northern California, to eastern Nevada. Deformation is consistent, within the 1 mm yr^{-1} uncertainties of the estimated site velocities, with a simple 10-parameter model using 6 rigid plates and 3 locked San Andreas system faults.

Introduction

We present a simple method for modeling crustal deformation as a combination of plate tectonic motions and interseismic elastic strain accumulation on faults. We assume the crust is composed of spherical caps, such as the major tectonic plates and microplates, that behave over many earthquake cycles as rigid bodies with angular velocity relative motions. Transient strain accumulation effects are accommodated by adding slip opposite the long-term rates (backslip) on the shallow seismogenic (locked) parts of the plate-boundary faults. Strain effects due to shallow backslip become negligible in the stable plate interiors where angular velocity motions predominate.

This method provides a better kinematic description of broadscale deformation than models using forward slip on semi-infinite deep faults [Savage and Burford, 1973], or other backslip dislocation models developed for subduction and strike-slip zones [Savage, 1983; Matsu'ura *et al.*, 1986] that assume block motions on planar surfaces, which do not approach angular velocities far from the plate boundaries.

We applied this method to Global Positioning System (GPS) measurements collected in Nevada and northern California that have sufficient precision and distribution to infer Pacific-North America plate boundary deformation at both tectonic plate and near-fault spatial scales.

Data Analysis

We analyzed continuous GPS data collected on 2443 days at 35 stations, which operated for at least 0.9 years from November 1993 to July 2000, by the Bay Area Regional Deformation (BARD) network in northern California [Murray *et al.*, 1998], the northern Basin and Range (NBAR) network in Nevada and eastern California [Bennett *et al.*, 1998], the International GPS Service (IGS), and other agencies (Fig. 1).

Uniform station velocities were estimated using GAMIT/GLOBK software and distributed processing methods [McClusky *et al.*, 2000]. We determined weakly constrained station positions for each day by tightly constraining IGS orbits and International Earth Rotation Service parameters, and station velocities by tightly constraining 3 IGS stations (ALGO, DRAO, FAIR) to their velocities in a “stable” North America plate (NA) reference frame [Kogan *et al.*, 2000].

The estimated velocities have 0.9–2.7 mm yr⁻¹ uncertainties. We assumed white-noise errors consistent with daily coordinate residual scatter, and 1 mm yr^{-1/2} colored-noise errors (e.g., monument wander), which typically range 0.5–2.0 mm yr^{-1/2} [Langbein and Johnson, 1997].

Deformation Model

We assume station velocity at geocentric position \mathbf{r} is

$$\mathbf{v}(\mathbf{r}) = \boldsymbol{\Omega}(\mathbf{r}) \times \mathbf{r} - \sum_{f=1}^F \mathbf{G} \cdot \mathbf{s}_f \quad (1)$$

where $\boldsymbol{\Omega}$ is the angular velocity vector, and strain effects are given by elastic Green's function \mathbf{G} responses to slip \mathbf{s} on F faults. Zones of distributed horizontal deformation can be described by letting $\boldsymbol{\Omega}(\mathbf{r})$ vary within the zones, and the latter terms can account for Earth sphericity [Pollitz, 1996] and viscoelastic response of the lower crust and upper mantle [Savage and Prescott, 1978].

To illustrate this approach, we here make several assumptions that, while limiting its general utility, simplify the model to an easily optimizable function. Angular velocities $\boldsymbol{\Omega} = \omega \hat{\boldsymbol{\Omega}}$, where ω is the angular rate of rotation and the unit vector $\hat{\boldsymbol{\Omega}}$ defines the Euler pole latitude and longitude, are assumed to be constant within each plate (i.e., rigid). We use rectangular dislocations [Okada, 1985] with backslip equal and opposite to the long-term slip rates to approximate strain due to shallow fully locked faults. Second-order effects due to Earth sphericity are assumed to be small near to faults where elastic strains are significant.

The study area is divided into 6 plates, based on seismic, geologic, and previous geodetic studies [Bennett *et al.*, 1999; Thatcher *et al.*, 1999; WG99, 1999] (Fig. 1, Table 1). Adjacent to the Pacific plate (PA), the San Andreas system in the San Francisco Bay area is represented by three strike-slip faults that bound the San Francisco (SF) and Martinez (MZ) plates. Station motions in the Bay Area are nearly parallel to the motion of PA relative to NA (denoted PA-NA) predicted by the NUVEL-1A Euler pole, denoted $\hat{\boldsymbol{\Omega}}_{PA}^{NU}$ [DeMets, 1994] (Figs. 1B and 2). Because the station distribution is insufficient to reliably estimate $\boldsymbol{\Omega}$ for the PA and Bay Area plates, we assume the observed strain can be described using dislocations that lie along small circles about $\hat{\boldsymbol{\Omega}}_{PA}^{NU}$ and estimate only ω for each plate. Fault locations and locking depths are assumed from surface geology and seismicity studies (Table 2) due to the high correlations typically observed between estimated fault geometry and slip parameters in a parallel fault regime [Freymueller *et al.*, 1999].

We use 2D (anti-plane strain) screw dislocations [Savage and Burford, 1973] to approximate strain due to parallel, locked faults in the Bay Area. In an x-y coordinate system, stations move parallel to a fault, which is located at $x=0$, locked from the surface to depth d , and slipping below at rate s , with velocity $v = \text{sgn}(x)s/2 - (s/\pi) \tan^{-1}(d/x)$ (cf. Eq. 1). For small-circle parallel velocities, the second term in Eq. 1 can be rewritten in terms of angular velocities and

angular distances ϕ from the Euler pole as

$$-\frac{a}{\pi} \sum_{f=1}^F \Delta\omega_f \sin \phi_f \tan^{-1} \frac{d_f}{a(\phi - \phi_f)} \quad (2)$$

where a is the Earth radius, and the distance from each fault located at ϕ_f is $a(\phi - \phi_f)$. Each fault has deep-slip rate $s_f = a\Delta\omega_f \sin \phi_f$, where $\Delta\omega_f$ is the difference in angular velocity rates on either side of the fault.

The Sierran-Great Valley plate (SG) is bounded by the San Andreas system and the NW-trending northern Walker Lane Belt (NWLB) of conjugate normal and strike-slip faults between Lake Tahoe and Mount Shasta. The Central Nevada Seismic Zone (CNSZ) of NE-trending normal faults divides the Basin and Range province (BR) into eastern (EB) and western (WB) plates. We confine EB-NA relative motion to the Intermountain Seismic Belt (ISB), including the east-west extensional Wasatch fault in Utah, which lies outside our network, and use the component of oblique SG motion parallel to Bay Area faults to determine $\Delta\omega_f$ across the SG-MZ boundary. The station distribution was not sufficient to reliably estimate the ISB, CNSZ, and NWLB locking depths.

Results

We estimated $\hat{\Omega}$ and ω for the SG, WB, and EB plates, and ω for the PA, SF, and MZ plates, with the latter pole locations constrained to $\hat{\Omega}_{PA}^{NU}$. The weighted residual χ^2 of 35 station horizontal velocities (70 components) used to estimate these 12 model parameters is 52.73. The estimated $\hat{\Omega}_{WB}$ (42.9°N, 115.8°W) is near $\hat{\Omega}_{EB}$ (42.9°N, 115.2°W). The χ^2 for a model constraining $\hat{\Omega}_{EB} = \hat{\Omega}_{WB}$ (i.e., a single BR pole location $\hat{\Omega}_{BR}$ with different angular rates for EB and WB) is 52.79. An F-ratio test shows the increase in χ^2 is significant at only the 3.2% confidence level, indicating that independent EB and WB poles are not required.

Horizontal station motions predicted by the preferred single $\hat{\Omega}_{BR}$ model (Table 1) have a total wrms misfit of 1.1 mm yr⁻¹. Misfits within each plate (Table 1) are comparable to the data uncertainties and consistent with plate rigidity. The χ^2 per degrees of freedom is 0.88, which is less than the expected value of 1.0, suggesting the colored-noise errors may be conservative. Assuming smaller errors for more deeply anchored stations, such as in NBAR [Wernicke et al., 2000], would improve detection of distributed deformation.

We assessed model uncertainties using bootstrap methods [Frey Mueller et al., 1999] due to the nonlinear pole location constraints. All ω are significantly greater than zero at 95% confidence (Table 1). The 2D-confidence regions of $\hat{\Omega}_{BR}$ and $\hat{\Omega}_{SG}$ are elongated due to the limited station distribution (Fig. 3). The direction of rotation of the SG, whose

pole uncertainty spans nearly 180°, is poorly resolved. $\hat{\Omega}_{SG}$ differs significantly from $\hat{\Omega}_{PA}^{NU}$ but is marginally consistent with $\hat{\Omega}_{BR}$, although other models combining one or more of the SG and BR Euler poles have significantly greater misfits at the 60–70% confidence level.

Discussion

Horizontal interseismic deformation in our study area is consistent, within the 1 mm yr⁻¹ uncertainties of the estimated site velocities, with a simple 10-parameter model using 6 rigid plates and 3 locked San Andreas system faults.

Predicted relative motions on the plate boundaries (Table 3) suggest that deformation across the Basin and Range can be partitioned into 2.4 mm yr⁻¹ east-west extension across the ISB, 2.3 mm yr⁻¹ east-west extension across the CNSZ, and 3.6 mm yr⁻¹ primarily right-lateral strike-slip on the NWLB. These results are in reasonable agreement with other GPS studies [Bennett et al., 1998; Bennett et al., 1999; Thatcher et al., 1999; Dixon et al., 2000]. Our observations in the BR lack sufficient precision and distribution to infer strain accumulation or detect zones of distributed deformation, as suggested by some of these studies.

The SG moves obliquely to the San Andreas system, with $\sim 2.4 \pm 0.4$ mm yr⁻¹ of fault-normal convergence (Table 3) being accommodated over a narrow (<15 km) zone (Figs. 1 and 2). This convergence, consistent with other GPS studies [Prescott et al., 2001], may contribute to uplift of the Coast Ranges [Argus and Gordon, 2001].

The inferred $\sim 37.2 \pm 1.0$ mm yr⁻¹ slip rate across the San Andreas system is consistent with geologic estimates based on the most active Holocene faults (Table 2). The slip rate on the Hayward fault is higher than the geologic estimate, although models with rates lower on the Hayward and higher on the other faults are also acceptable due to high correlations between these parameters.

The estimated ω_{PA} is significantly higher than the 3.16-Ma NUVEL-1A rate (0.749 ± 0.012° Ma⁻¹, Fig. 2), in agreement with DeMets and Dixon [1999]. Our assumed $\hat{\Omega}_{PA}^{NU}$ and estimated $\hat{\Omega}_{SG}$ significantly differ from other geodetic estimates (Fig. 3), possibly because we used only three stations to define “stable” NA. Preliminary analysis using a more globally distributed set of stations that allows direct estimation of $\hat{\Omega}_{PA}$ shows better agreement with other studies [DeMets and Dixon, 1999; Dixon et al., 2000].

The angular-velocity fault-backslip model provides a general framework for estimating long-term plate motions over regional and global scales using geodetic measurements subject to short-term earthquake-cycle effects. We have begun analyzing survey-mode GPS data to improve the spatial resolution of deformation, estimate locking on the other plate

boundary faults, and detect zones of distributed deformation. We are also modeling more complex, 3D fault systems by summing backslip on rectangular dislocations. This will allow us to include subduction zones and to estimate along-strike variations in locking on a geometrically more realistic model of the San Andreas fault system.

Acknowledgments.

We thank R. Bennett, T. Dixon, A. Lowry, and an anonymous referee for constructive reviews. We thank W. Prescott, B. Romanowicz, and the staffs of the Berkeley Seismological Laboratory and U.S. Geological Survey for help maintaining the BARD network. We thank the many other individuals and institutions responsible for maintaining the other networks and data products, including the IGS, NOAA, FAA, JPL, Caltech, Scripps Institution of Oceanography, and Harvard-Smithsonian Center for Astrophysics. The work was supported by the National Earthquake Hazards Reduction Program and the National Science Foundation. The figures were made using the public domain GMT software. Station velocities are available at <http://quake.geo.berkeley.edu/bard>.

References

- Argus, D. F., and R. G. Gordon, Present tectonic motion across the Coast Ranges and San Andreas fault system in central California, *Geol. Soc. Am. Bull.*, in press, 2001.
- Bennett, R. A., B. P. Wernicke, and J. Davis, Continuous GPS measurements of contemporary deformation across the northern Basin and Range province, *J. Geophys. Res.*, *25*, 563–566, 1998.
- Bennett, R. A., J. L. Davis, and B. P. Wernicke, Present-day pattern of Cordilleran deformation in the western United States, *Geology*, *27*, 371–374, 1999.
- DeMets, C., Effect of recent revisions to the geomagnetic reversal time scale on estimates of current plate motions, *Geophys. Res. Lett.*, *21*, 2191–2194, 1994.
- DeMets, C., and T. H. Dixon, New kinematic models for Pacific-North America motion from 3 Ma to present, I: Evidence for steady motion and biases in the NUVEL-1A model, *Geophys. Res. Lett.*, *26*, 1921–1924, 1999.
- Dixon, T. H., M. Miller, F. Farina, H. Z. Wang, and D. Johnson, Present-day motion of the Sierra Nevada block and some tectonic implications for the Basin and Range province, North American cordillera, *Tectonics*, *19*, 1–24, 2000.
- Freyemueller, J. T., M. H. Murray, P. Segall, and D. Castillo, Kinematics of the Pacific-North America plate boundary zone, northern California, *J. Geophys. Res.*, *104*, 7419–7442, 1999.
- Kogan, M. G., G. M. Steblov, R. W. King, T. A. Herring, D. I. Frolov, S. G. Erorov, V. Y. Levin, A. Lerner-Lam, and A. Jones, Geodetic constraints on the rigidity and relative motion of Eurasia and North America, *Geophys. Res. Lett.*, *27*, 2041–2044, 2000.
- Langbein, J., and H. Johnson, Correlated errors in geodetic time series: Implications for time-dependent deformation, *J. Geophys. Res.*, *102*, 591–603, 1997.
- Matsu'ura, M., D. D. Jackson, and A. Cheng, Dislocation model for aseismic crustal deformation at Hollister, California, *J. Geophys. Res.*, *91*, 2661–2674, 1986.
- McClusky, S., et al., Global Positioning System constraints on plate kinematics in the eastern Mediterranean and Caucasus, *J. Geophys. Res.*, *105*, 5695–5719, 2000.
- Murray, M. H., R. Bürgmann, W. H. Prescott, B. Romanowicz, S. Schwartz, P. Segall, and E. Silver, The Bay Area Regional Deformation (BARD) permanent GPS network in northern California, *EOS Trans. AGU*, *79*, F206, 1998.
- Okada, Y., Surface deformation due to shear and tensile faults in a half-space, *Bull. Seismol. Soc. Am.*, *75*, 1135–1154, 1985.
- Pollitz, F. F., Coseismic deformation from earthquake faulting on a layered spherical Earth, *Geophys. J. Int.*, *125*, 1–14, 1996.
- Prescott, W. H., J. C. Savage, J. L. Svarc, and D. Manaker, Deformation across the Pacific-North America plate boundary near San Francisco, California, *J. Geophys. Res.*, *106*, 6673–6682, 2001.
- Savage, J. C., A dislocation model of strain accumulation and release at a subduction zone, *J. Geophys. Res.*, *88*, 4984–4996, 1983.
- Savage, J. C., and R. O. Burford, Geodetic determination of relative plate motion in central California, *J. Geophys. Res.*, *78*, 832–845, 1973.
- Savage, J. C., and W. H. Prescott, Asthenosphere readjustment and the earthquake cycle, *J. Geophys. Res.*, *83*, 3369–3376, 1978.
- Thatcher, W., G. R. Foulger, B. R. Julian, J. Svarc, E. Quilty, and G. W. Bawden, Present-day deformation across the Basin and Range province, western United States, *Science*, *283*, 1714–1718, 1999.
- Wernicke, B., A. M. Friedrich, N. A. Niemi, R. A. Bennett, and J. L. Davis, Dynamics of plate boundary fault systems from Basin and Range Geodetic Network (BARGEN) and geologic data, *GSA Today*, *10(11)*, 1–7, 2000.
- WG99, Earthquake probabilities in the San Francisco Bay region: 2000 to 2030—A summary of findings, *USGS Open File Rpt.*, *99-417*, 1999.
- M. H. Murray, Berkeley Seismological Laboratory, 215 McCone Hall, University of California, Berkeley, CA 94720-4760. (e-mail: mhmurray@seismo.berkeley.edu)
- P. Segall, Geophysics Dept., Stanford Univ., Stanford, CA 94305-2215. (e-mail: segall@pangea.stanford.edu)

Received May 2, 2001; revised August 31, 2001; accepted September 5, 2001.

¹Now at Seismological Laboratory, Univ. of Calif., Berkeley

Table 1. Best-fitting Angular Velocities

	Plate	Lat., °N	Lon., °W	ω , ° Ma ⁻¹	Misfit, mm yr ⁻¹
PA	Pacific	48.7	78.2	0.774 ^{+0.007} _{-0.043}	1.1
SF	San Francisco	48.7	78.2	0.489 ^{+0.071} _{-0.040}	1.4
MZ	Martinez	48.7	78.2	0.258 ^{+0.033} _{-0.080}	1.0
SG	Sierran-GV	53.9	90.1	0.208 ^{+0.280} _{-0.115}	1.1
WB	Western BR	43.2	115.3	0.588 ^{+0.271} _{-0.357}	0.3
EB	Eastern BR	43.2	115.3	0.285 ^{+0.138} _{-0.218}	1.1

Angular velocities relative to NA. Rates ω are left-hand rotations (clockwise reckoned positive) with 95% confidence intervals. Model: $\hat{\Omega}_{PA} = \hat{\Omega}_{SF} = \hat{\Omega}_{MZ} \equiv \hat{\Omega}_{PA}^{NU}$ and $\hat{\Omega}_{WB} = \hat{\Omega}_{EB} \equiv \hat{\Omega}_{BR}$. BR = Basin and Range province, GV = Great Valley.

Table 2. San Andreas Fault System

Fault	Angular Dist., °	Depth, km	Slip, mm yr ⁻¹	
			GPS	Geol.
SA San Andreas	33.6772	12.0	17.5 ^{+5.4} _{-2.8}	17±4
H Hayward	33.4180	8.5	14.2 ^{+3.6} _{-8.4}	9±2
CC Concord/Calav.	33.2104	10.4	5.5 ^{+5.3} _{-2.7}	6±2
Total			37.2 ^{+2.8} _{-1.3}	41±6

Angular distance relative to $\hat{\Omega}_{PA}^{NU}$. Depth of locking from surface. Slip rates with 95% confidence intervals: GPS, preferred model; Geologic, [WG99, 1999]. Total geologic rate includes San Gregorio and Greenville faults (7 ± 4 , 2 ± 1 mm yr⁻¹, respectively).

Table 3. Plate Boundary Deformation

Plates	Boundary	Lat., °N	Lon., °W	Rate, mm yr ⁻¹	Az., °N
EB-NA	ISB	40.00	111.80	2.4 ^{+1.1} _{-1.4}	234
WB-EB	CNSZ	40.00	118.00	2.3 ^{+1.3} _{-1.1}	300
SG-WB	NWLB	40.00	121.00	3.6 ^{+1.4} _{-0.8}	309
MZ-SG	Coast Range	38.08	122.05	2.4 ^{+0.9} _{-0.9}	237

Relative motions, which vary along boundaries, at selected locations. Coast Range is fault-normal convergence across CC. Rates have 95% confidence intervals. Plates and boundaries, see Fig. 1.

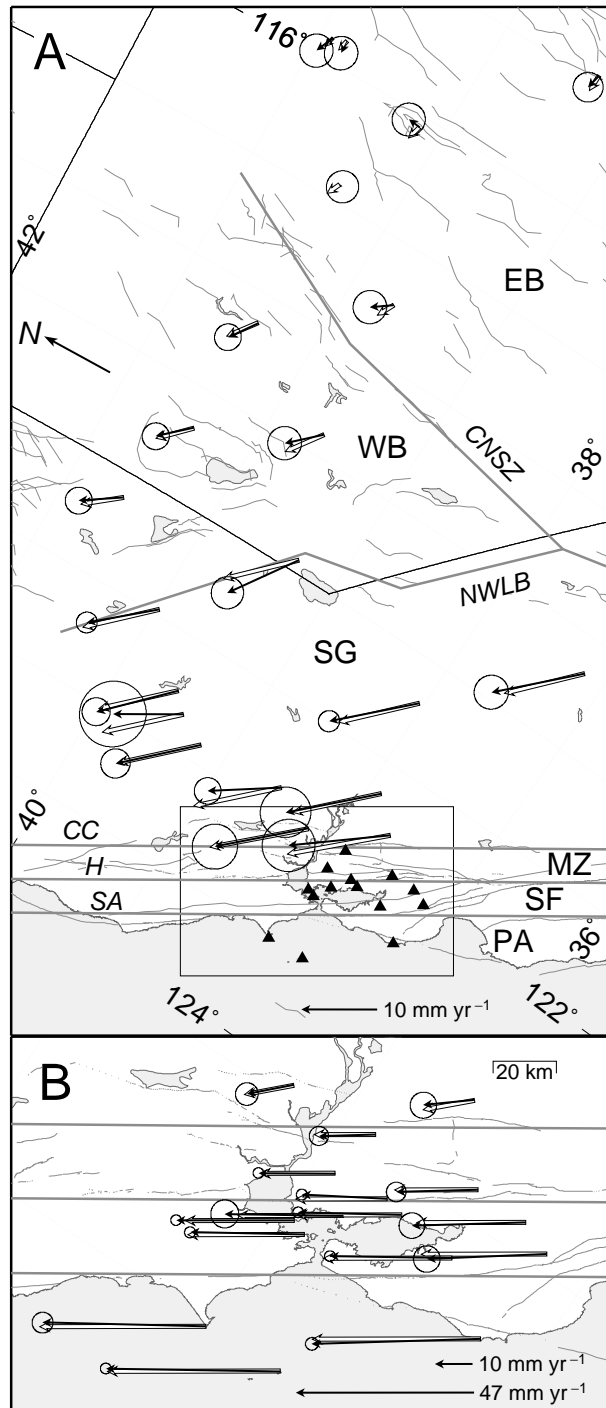


Figure 1. Predicted (open) and observed (solid) site velocities, with 95% confidence regions, relative to NA. Projection, oblique Mercator about $\hat{\Omega}_{PA}^{NU}$. A) northern California and Nevada (see box in Fig. 3), with velocities of sites in box (triangles) omitted for clarity. B) San Francisco Bay area. Plates given in Table 1. Faults: SA = San Andreas, H = Hayward, CC = Concord/Calaveras, NWLB = northern Walker Lane Belt, CNSZ = Central Nevada Seismic Zone.

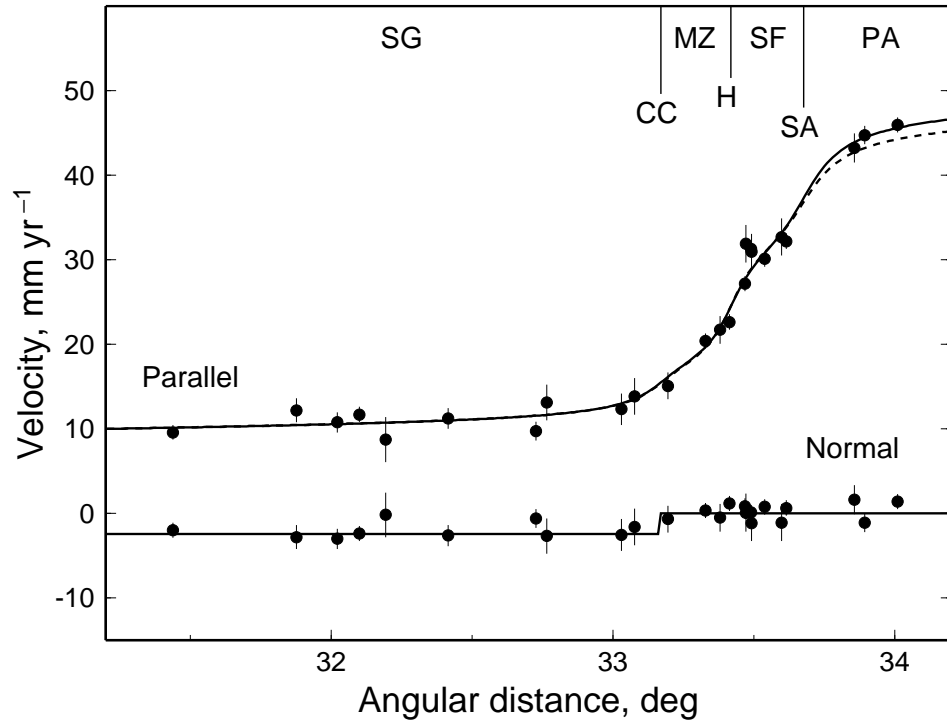


Figure 2. Velocities relative to NA, with one standard error bars, parallel and normal to small circles about $\hat{\Omega}_{PA}^{NU}$ versus angular distance from $\hat{\Omega}_{PA}^{NU}$. Solid line, preferred model. Dashed line, $\omega_{PA} = \omega_{PA}^{NU}$ model with significantly greater misfit (95% confidence) than preferred model. Plate regions and San Andreas faults are shown schematically at top.

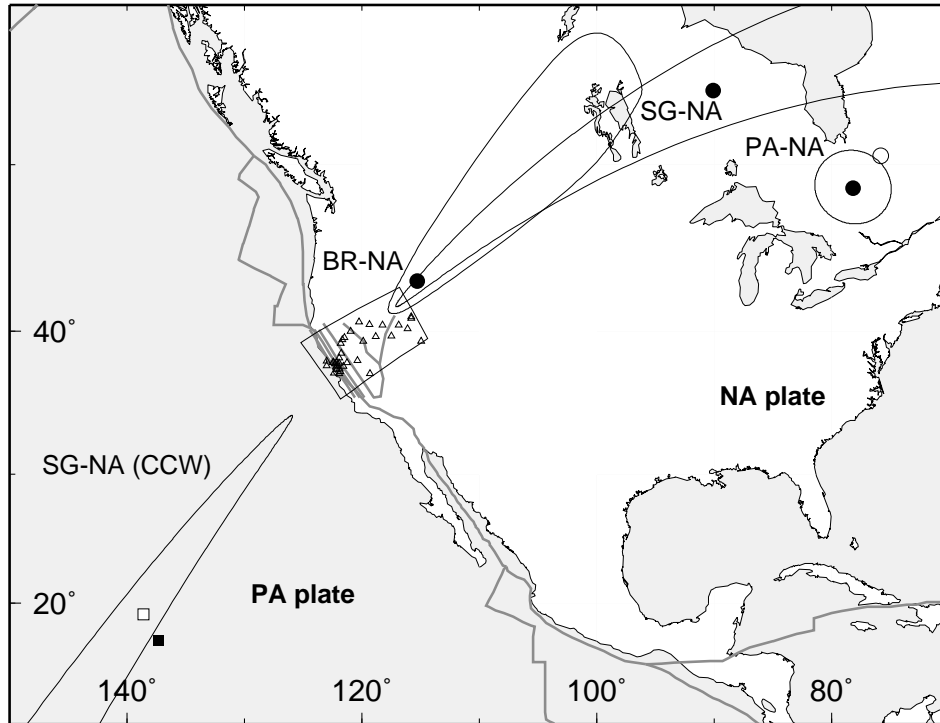


Figure 3. Estimated $\hat{\Omega}$ (solid circles) with 95% confidence bootstrap regions. PA-NA is $\hat{\Omega}_{PA}^{NU}$. Open circle, alternative $\hat{\Omega}_{PA}$ [DeMets and Dixon, 1999]. BR-NA applies to both WB and EB. The SG-NA uncertainty, which spans nearly 180°, has both clockwise (top) and counterclockwise (bottom) rotation regions, and includes pure translation (Euler pole at 90° distance from SG). Squares, alternative $\hat{\Omega}_{SG}$: open, [Argus and Gordon, 2001]; solid, [Dixon et al., 2000]. Box encloses stations and plate boundaries shown in Fig. 1.